journal

J. Am. Ceram. Soc., 83 [3] 578–84 (2000)

Effects of Pores on Mechanical Properties of Plasma-Sprayed Ceramic Coatings

Toshio Nakamura,† G. Qian,† and Christopher C. Berndt*,‡

Department of Mechanical Engineering and Department of Materials Science and Engineering, State University of New York at Stony Brook, Stony Brook, New York 11794

The effects of pore sizes, shapes, and orientations on the mechanical properties of thermally sprayed ceramic coatings are investigated. The analysis is conducted using detailed finite-element models with geometries similar to those of actual ceramic coatings containing many embedded pores. These microstructural models include many randomly placed pores of different sizes and shapes and are loaded in tension to determine their effective elastic moduli along the spray and transverse directions. We modeled coatings with statistical distributions of pore sizes and shapes that followed those of actual Al_2O_3–TiO_2 coatings. Because the pores in such a model are of different sizes and shapes, the model must be large enough to contain sufficient pores before the average modulus obtained from uniaxial loading can be identified as an effective property. Using differently sized models, we determined the variability of the average moduli. Such information is valuable when homogenized or continuum material models are used in the stress analyses of coatings. Our computed results show that a model must be large enough to contain 50–100 pores before the averaging of properties is accurate. Using the Al_2O_3–TiO_2 models, we also simulated microindentation tests. Unlike the results determined from uniaxial loading, the elastic moduli estimated from indentation possessed large variations. Apparently, the morphology of the pores immediately beneath the indentation or within the zone of influence has a significant effect on the response of the indenter and the measured modulus. The implications of these results and the computational capability to predict the mechanical properties of porous, plasma-sprayed ceramic coatings are discussed here.

I. Introduction

THE microstructure of a thermally sprayed ceramic coating is characterized by the existence of various pores, microcracks, splat boundaries, and unmelted particles. These attributes greatly influence the overall, or so-called effective, mechanical properties of coatings. In general, an inhomogeneous microstructure reduces the overall stiffness, coating strength, and integrity. Thermally sprayed coatings also are anisotropic, adding complexity to their mechanical characterization. Numerous experiments have measured the effective, or average, properties of coatings. For plasma-sprayed coatings, the measured values of coatings made with the same feed materials have shown large variation, depending on the fabrication processes. Also, measurements have yielded inconsistent results, even with similar specimens. In the present work, we attempt to identify sources of inconsistency through the investigation of microstructural models. Such analysis requires a novel method to model key microstructural factors of the coatings and to predict the effective response of the coatings quantitatively. The determination is not possible from available analytical models.

In this study, models closer to the microstructures of coatings are developed, using many randomly distributed pores with various sizes and shapes. Although this procedure is similar to many computational analyses conducted to determine the effective properties of composites reinforced with fibers and particles, there is a fundamental difference: A thermally sprayed coating contains no two pores exactly alike. This geometric feature implies the absence of symmetry and repeatability conditions that are used in many composite analyses. Modeling many pores to develop an accurate representation of coatings greatly increases the complexity of the analysis. Although notable microstructural features include splat boundaries and inhomogeneous phases, the only microstructural feature considered here is pores.

To study closely the properties of actual coatings, we modeled ceramic coatings with statistical distributions of pore sizes and shapes that followed those of Al_2O_3–TiO_2 coatings.[1] We attempted to determine the minimum model/domain dimensions to obtain a consistent modulus. Understanding these dimensions is valuable when the properties are homogenized and continuum models are used in stress and deformation analyses. Homogenized models assume that a microstructural length scale (e.g., pore size) is much smaller than a structural size scale (e.g., coating thickness). We investigated the validity of such an assumption for plasma-sprayed coatings.

In recent years, microindentation has been widely used to measure the hardness as well as the effective elastic modulus of a thin ceramic coating, because the method is versatile and easy to use. In the present study, the indentation tests are simulated, and coating moduli are estimated based on the Hertz contact theory. These values are compared with the effective moduli determined from the uniaxial tension of the models. The results reveal the source of inconsistent results obtained in indentation tests.

II. Microstructure of Plasma-Sprayed Coatings

The process of plasma spraying renders unique coating microstructures, which are very different from those of corresponding bulk materials. The coating microstructures can be summarized as porous lamellar structures, as shown in Fig. 1. The pancake-shaped splat, ~1–5 μm thick and 10–50 μm in diameter, is the basic structural unit of a coating.[2] Inside a splat, perpendicular columnar grain structures indicate the gradient direction of the solidification process. Because of the nature of the thermal spraying process, various types of defects are observed in coatings.[3,4] Those defects may lie along splat boundaries and are caused by weak adhesion between splats. The vertical microcracks usually initiate from the low-adhesion grain boundaries or from some initial defects within splats. They are believed to be generated by quenching and subsequent stress relaxation during the cool-down process. These sharp delaminations and microcracks may grow under certain mechanical and/or thermal loads and weaken coatings. Although

K. T. Faber—contributing editor

Manuscript No. 189696. Received December 14, 1998; approved August 20, 1999.
Supported by the Center for Thermal Spray Research at Stony Brook, under Grant No. NSF-MRSEC DMR632570.
*Member, American Ceramic Society.
†Department of Mechanical Engineering.
‡Department of Materials Science and Engineering.

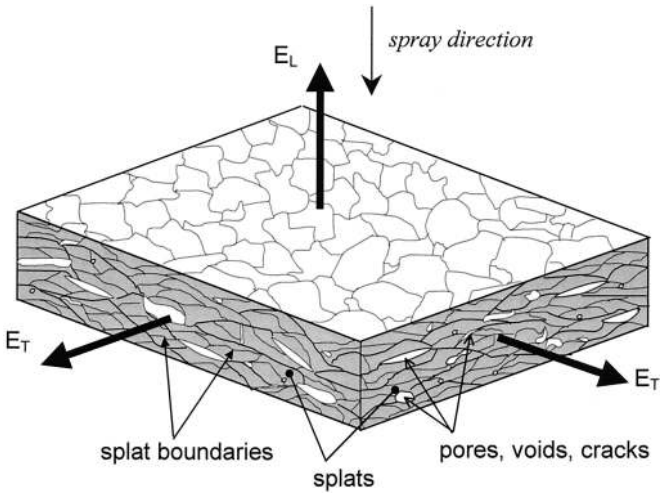

Fig. 1. Schematic of microstructure of plasma-sprayed ceramic coating (directions of elastic moduli along spray direction (E_L) and transverse direction (E_T) are indicated by heavy arrows).

different terms such as *void*, *delamination*, and *microcrack* are used above, their difference lies mostly in their aspect ratios (ratio of the major axis over the minor axis). Thus, we do not distinguish among them in terminology in this paper, and all are collectively treated as pores.

Numerous experiments have been conducted to evaluate the porosity of thermally sprayed coatings. Depending on the coating process and spray parameters, the porosity or the total volume fraction of pores in ceramic coatings may range from less than a few percent to ~20%. The layered microstructure, weak horizontal splat boundaries, and vertical microcrack growth caused by internal stress relaxation lead to horizontally and vertically oriented long, sharp pores. Consequently, the horizontal and vertical directions are the preferred pore orientations, resulting in the anisotropy observed in coatings.

III. Methods for Estimating Effective Properties

The global, or average, properties of plasma-sprayed coatings usually are very different from those of fully dense materials. The effective elastic modulus of ceramic coatings can be measured by various experimental methods, such as uniaxial-tension, four-point-bend, indentation, and ultrasonic tests. Because of the microstructure of ceramic coatings, their moduli can be a small fraction of the intrinsic modulus. Pores and splat boundaries constitute major reductions of the modulus. In addition, inhomogeneous phases, impurities, and residual stresses probably contribute to lowering the elastic constants.

In general, a higher porosity or void volume fraction leads to a lower elastic modulus. At the same time, porosity is needed for a higher thermal-insulation effect. Thus, it is desirable to determine an optimal pore distribution that minimizes thermal conductivity without making the coatings very compliant. Because of their microstructure, coatings often are modeled as a transversely isotropic material at the macroscale level. Numerous efforts have been made to evaluate the effective elastic constants of porous and cracked media.[5–9] Those analyses result in two categories: noninteracting and interacting models. The first model is based on the assumption that neighboring pores do not influence the deformation of one another and that the overall effect can be obtained by the summation of effects from the individual pores. This noninteraction assumption is accurate only when porosity is low. Several approximate methods have been developed to evaluate the effective properties of the interacting pore and crack problems of the second model. Some common methods are the self-consistent, differential, and Mori–Tanaka schemes.[10,11]

Zhao *et al*.[5,6] have presented a hybrid approximate method that combines the Mori–Tanaka method and Eshelby's solution for an ellipsoidal inclusion to solve for the effective mechanical properties of an ellipsoidal array in porous media. For materials with elliptical pores, the two-dimensional elastic moduli in the spray, or longitudinal, direction, E_L, and the transverse direction, E_T, can be estimated as[6,8]

$$E_L = \frac{E_m(1-p)}{1+2\pi\rho} \tag{1a}$$

$$E_T = \frac{E_m(1-p)}{1+2\pi\rho\alpha^{-2}} \tag{1b}$$

Here, E_m is the matrix modulus, p the porosity, ρ ($=\Sigma\, a_i/A$) the crack density, and α ($=(\Sigma\, a_i^2/\Sigma\, b_i^2)^{1/2}$) the average pore aspect ratio, where A is the total area and a_i and b_i the major and minor axes, respectively, of ith pore.

The analytical approaches are valid for estimating the effective modulus of solids containing many pores. Thus, a required number of pores must exist within a domain or model to produce a consistent effective modulus. Intuition says that this domain must be large with respect to the characteristic pore sizes, in order to contain sufficient pores. In fact, the minimum domain size must be known in order to treat a coating as a homogeneous material with an average/effective modulus as its property. For pores with uniform size, the domain size should be about one order larger than the pore size. However, the required dimension is not yet obvious for pores with various sizes and shapes found in sprayed coatings. In the present study, this dimension is determined by studying variations of average moduli obtained from many models with various pore morphologies.

IV. Coatings with Many Pores

(1) Random Pore Size, Shape, Orientation, and Location

Simulation of the unique microstructures of a plasma-sprayed coating requires a model that allows for random distributions of numerous pores with various sizes and aspect ratios. Within the model, pores are placed at random locations. Furthermore, every pore is assumed to possess three additional geometric attributes: pore size/area, pore shape or aspect ratio, and pore orientation with respect to the spray or transverse direction. The phrase random model is used here to denote this type of modeling. Precisely, the random model is the result of four separate pore attributes. The first attribute is the pore location, which is randomly determined; the second includes the various selections of pore sizes; and the third is the randomly chosen pore aspect ratio. The fourth attribute consists of the nonregular orientations of pores. All of these parameters are nonuniformly assigned to each pore in the random models. A computational program has been developed to generate a series of finite-element models that simulate coatings with such random attributes.

In order to guarantee that a coating model represents the constitutive response of a coating, the model must contain sufficient pores. Based on past experience[12] and trial calculations, we estimate that models with a few hundred pores would require a very large number of finite elements. To minimize the cost, we have adopted an idealized computational strategy. First, a random model is divided into many small regions, which may or may not contain a pore. The selection of regions that contain pores is made through a stochastic process, to generate random numbers. The process is repeated as many times as necessary to generate enough pores to satisfy a desired porosity.

Sizes and shapes of pores also are determined through a similar stochastic process. However, to make this process more systematically and computationally effective, we impose limits for the area and aspect ratio of the pore. First, all of the pore shapes are idealized to be hexagonal. The size/area is assumed to range from A_{min} to $10A_{min}$, where A_{min} is chosen to be ~1/50 the area of the subregion. Any pores with less area have little influence on the overall properties. Also, the aspect ratios of pores are set to vary from $a/b = 1$ to $a/b = 10$. Furthermore, instead of allowing

continuous variations in the area and the aspect ratio, we use five distinct pore areas, $A/A_{min} = 1, 2, 4, 6$, and 10, and five aspect ratios, $a/b = 1, 2, 4, 6$, and 10. Therefore, there are 25 possible types of pores, varying in area and shape. Categorizing pores into 25 types enables us to assign various weight factors to the pore types. In the initial random-model analysis, the weights are set randomly, but in the subsequent analysis, where pore size and shape distributions are set according to Al_2O_3–TiO_2 coatings, each pore type is assigned a certain weight to satisfy the predetermined distributions. In addition to having various shapes and sizes, every pore is rotated by some amount. Here, the orientation angle of a given pore is prescribed to range randomly within $-20°$ to $20°$. Such a range of rotation conforms to the observed inclined angles of most pores.[1] Additionally, to reduce the uniformity associated with the hexagonal array, we slightly translate each pore from the centroid of each region. The direction and magnitude of the shift are arbitrary, but they are restricted by the boundaries and the shape requirements for the finite elements. A typical random model generated according to the present scheme is shown in Fig. 2.

The present analysis showed that the mesh design has a significant effect on computational accuracy. Deformation caused by a high stress concentration near every pore tip clearly must be captured to obtain a proper coating response. We tested several mesh designs to improve the accuracy of the random model. With the mesh arrangements shown in the inset of Fig. 2, we were able to minimize the discretization error. A total of ~12 000 elements were used to construct a single random model. All of the elements were chosen to be four-noded, generalized plane-strain elements that allow uniform out-of-plane deformation. The four sides of the random models are constrained to be straight. In the first phase of the random-model analysis, distributions of pore sizes and shapes are assumed to be arbitrary. Thus, one model may contain more cracklike pores (e.g., $a/b = 10$), whereas another model may have more circular pores (e.g., $a/b = 1$). Alternatively, two random models of similar porosity may show quite different overall mechanical responses. These models were used to determine the effective elastic moduli along the spray direction, E_L, and the transverse direction, E_T, under uniaxial loading conditions.

(2) Effective Moduli of Random-Pore Models

In order to obtain statistically meaningful results, we constructed 45 separate random models, with overall porosities ranging from ~2% to 10%. Computed effective elastic moduli, E_L and E_T, were normalized with the matrix or pore-free modulus, E_m, and are shown in Fig. 3. Poisson's ratio was set to $\nu_m = 0.25$ in all cases. Although the other material constants, such as Poisson's ratios, were computed and shown to vary with porosity,[13,14] only the results for E_L and E_T are presented here because of space constraints. A general trend revealed by the figure is that both moduli decrease as porosity increases. However, for the spray-direction modulus, the results are scattered at any given level of porosity. Our random models predict the spread of the modulus in the spray direction to be as high as 25% for a porosity >5%. The basic reason for the scatter is that every model has a different average aspect ratio or pore shape. Even with 400 pores, randomly determined aspect ratios produce different average values and result in scattering of the estimated E_L. Interestingly, such scatter is much lower for the transverse modulus. This observation confirms that porosity alone is not accurate for characterizing the effective modulus. In fact, a ceramic coating with a higher porosity may have a higher modulus than one with a lower porosity. These results also are consistent with the experimentally measured elastic modulus.

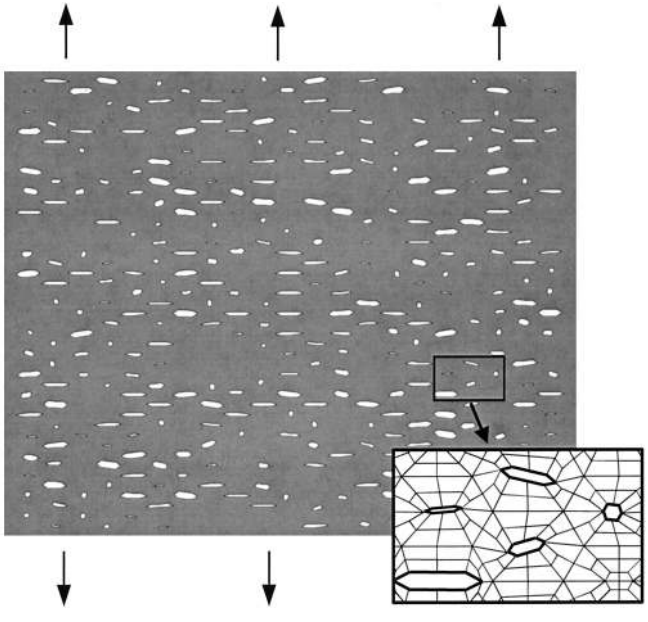

Fig. 2. Typical sprayed-coating model, with randomly shaped, sized, and distributed pores; pores were subjected to a uniform tensile load to measure effective elastic modulus (small region of finite-element mesh is enlarged in inset).

V. Models for Alumina–Titania Coatings

(1) Statistical Distributions of Pore Sizes and Shapes

Experimentally measured pore-size and shape distributions of a plasma-sprayed coating can provide insight into the relationship between plasma-spray processes and coating microstructural details as well as the basis for simulating coating microstructures and studying how coating microstructures affect mechanical and thermal properties. Some precise quantitative studies have been made of pore sizes and shapes in coatings, using various techniques, including X-ray tomography.[15] Here, our aim is not to precisely model a small section of a coating with a few pores but rather to identify underlying geometric factors that characterize the overall mechanical response. For this purpose, collective information on many pores is needed, rather than very accurate descriptions of a few pores. Such results are available from the stereologically measured data obtained by Leigh and Berndt,[1] a complete set of data on the pore size and shape distributions found in a plasma-sprayed Al_2O_3–13 wt% TiO_2 coating. According to the measurements, the sizes of most pores fall between 3 and 10 μm, and sharp, cracklike pores are abundant in the Al_2O_3–TiO_2 coating.

In fact, many of the larger-sized pores were cracklike, whereas most small pores were close to circular in shape. The total porosity of the coating, measured by the Archimedes method, was ~9.1%. For the Al_2O_3–TiO_2 models, the pore-free modulus was chosen from the nanoindentation test data. Nanoindentation is designed to

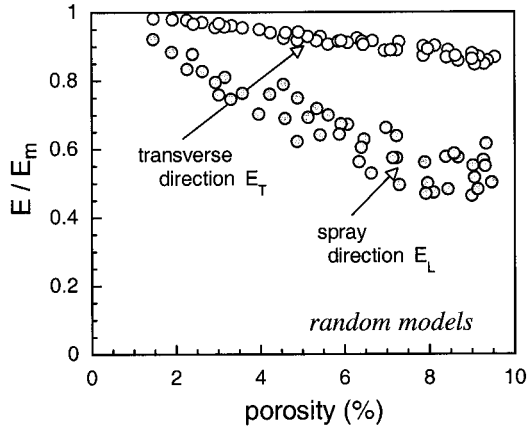

Fig. 3. Effective elastic moduli of random models with various pores, normalized by the matrix modulus (E_m) and shown as a function of porosity. Each circle represents a modulus of an individual coating model; there are 48 independent models ((●) spray-direction (E_L) moduli and (○) transverse-direction (E_T) moduli).

measure the elastic modulus of a single splat.[16] The depth of a nanoindenter penetration is only ~100–500 nm, and it is assumed that such a small indentation depth is insufficient to include the modulus reduction by pores. The splat elastic modulus of the as-sprayed Al_2O_3–TiO_2 coating measured by the nanoindentation test was 180 GPa.[1] Although the bulk elastic modulus of the Al_2O_3–TiO_2 was much higher, splat boundaries, impurities, and other factors unique to thermally sprayed coatings contributed to the low modulus. Poisson's ratio was kept at $\nu_m = 0.25$. Various experiments were conducted to measure the moduli of as-sprayed Al_2O_3–TiO_2 using indentation, four-point-bend, and flexural-vibration tests. The experimentally measured modulus in the spray direction ranged from 38 to 70 GPa.[17–19]

(2) Various Domain Sizes

In many coating analyses at the structural level, the coatings are idealized as homogeneous and continuum materials. However, in order to use the effective, or average, properties in material models, structural size scales (e.g., coating thickness) of interest must be much larger than microstructural length scales (e.g., pore size). Quantitatively, the structural size scale should be at least several multiples of domain size before a consistent average modulus can be obtained. Using the models for Al_2O_3–TiO_2, we estimated the size of such a domain. For randomly distributed pores with uniform size, a nearly consistent effective modulus should be obtained once the domain size is about an order of magnitude larger than the pore diameter. However, such a size requirement is yet to be determined for pores of different shapes and sizes.

In order to determine the minimum domain size, the pore size and shape distributions of Al_2O_3–TiO_2 were used to construct computational models in three different domain sizes, as shown in Fig. 4. The small domain measured 90 μm × 100 μm and contained an average of ~32 pores. The medium domain measured 170 μm × 200 μm and contained an average of ~135 pores. The large domain measured 370 μm × 300 μm and contained an average of ~450 pores. For each domain size, 10 separate models were constructed, using the model and mesh generator program. Although the pores of all of the models were set to follow statistically the Al_2O_3–TiO_2 pore size and shape distributions, actual distributions in the small models had some variations, because there were insufficient pores to represent the distributions

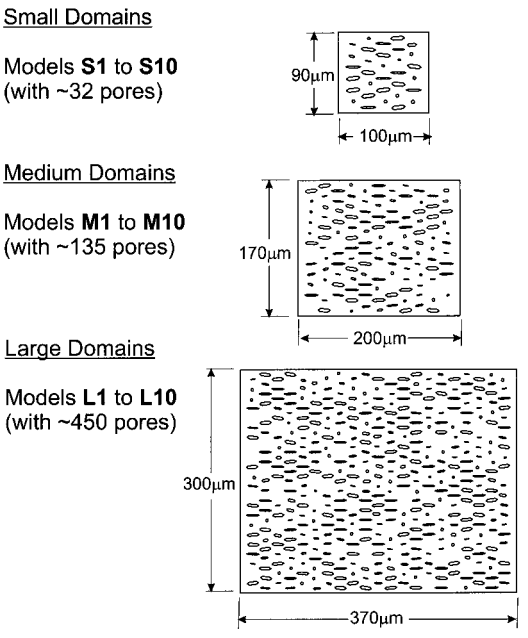

Fig. 4. Illustrations of domains with three different overall sizes (small, medium, large) for Al_2O_3–TiO_2 coating; for each domain size, 10 separate models were constructed (domains are not drawn in exact proportions).

precisely. However, all of the models were prescribed to have a porosity of $p = 9.10 \pm 0.15\%$ and a mean aspect ratio of $\alpha = 4.80 \pm 0.15$. According to the analytical formula of Eq. (1), the estimated moduli were $E_L = 87$ GPa and $E_T = 158$ GPa under these porosities and aspect ratios.

(3) Estimated Moduli of Alumina–Titania Coating

The models were loaded in uniaxial tension, and the load-elongation relations were used to obtain their effective elastic moduli. The normalized moduli along the spray direction, as well as along the transverse direction, for each domain size are shown in Fig. 5. In each different domain size, the average values from the 10 models were very close at $E_L \approx 84$ GPa, which is slightly lower than the analytical result. However, there were some variations in the computed E_L values for the small domains (*S*1–*S*10); those of the larger domains were more consistent. The standard deviations were 3.9, 2.2, and 0.6 GPa for the small, medium, and large domains, respectively. On the other hand, for the modulus along the transverse direction, all of the models fell within 0.5% of the mean value, $E_T = 157.6$ GPa, regardless of the domain size.

Two major observations can be made here. First, once the detailed size and pore distributions were prescribed, unlike in the random-model results shown in Fig. 3, the scattering of moduli disappeared, as long as the models contained many pores (see Fig. 3(c)). Second, there were some variations in E_L when the domain was small; the variability diminished for larger domains. Although there was no clear transition, the domain size dependence seemed less than ±5% when the size was ~150 μm × 150 μm. For the Al_2O_3–TiO_2, such a domain contained ~90 pores. Because the largest pores in the model were ~18 μm, that domain was about eight times longer. A more restrictive variability (e.g., 1%–2%) for the domain size independence would require greater domain sizes (e.g., ~300 μm). Compared with the experimentally determined modulus (e.g., microindentation), these results were somewhat higher. This discrepancy is attributed to the fact that very long pores with a high aspect ratio (i.e., cracklike) could not be modeled here. The presence of such pores in actual coatings would further reduce the stiffness.

VI. Simulations of Microindentation Tests

(1) Computational Procedure

Microindentation tests are used increasingly to measure various mechanical properties of coatings. The indentation techniques have been widely used to determine hardness as well as elastic modulus and fracture toughness. The strength of these techniques lies in their versatility and relative simplicity for measuring the properties. There are several types of indentation tests, including Knoop and spherical-indentation techniques.[15] In order to gain insights into the indentation mechanisms and processes, we investigated the microindentation of the Al_2O_3–TiO_2 models using a round indenter. Our analysis was based on the model for Hertzian contact theory, and a finite-element model with a semicircular indenter being contacted and pressed onto an Al_2O_3–TiO_2 coating is described here. The relationship between the contact force and the indented displacement depends on the indenter radius, the elastic moduli of the indenter and coating, and the magnitude of the force. From the measured displacement and contact force record, one can estimate the coating modulus. In many experiments, the modulus is obtained from the elastic unloading curve.

For the coating, we selected the six large domain models described in the previous section (Models *L*1 to *L*6). We also chose an indenter diameter of 100 μm and set its modulus very high, so that the indenter could be considered rigid. In the finite-element simulations, the contact conditions were imposed along the top surface of the coating and the round indenter. In order to minimize any error arising from finite-element discretization, we initially conducted the contact analysis on homogeneous models with no pores. These models had mesh designs similar to those of the models with pores. Using the solutions of these models, we

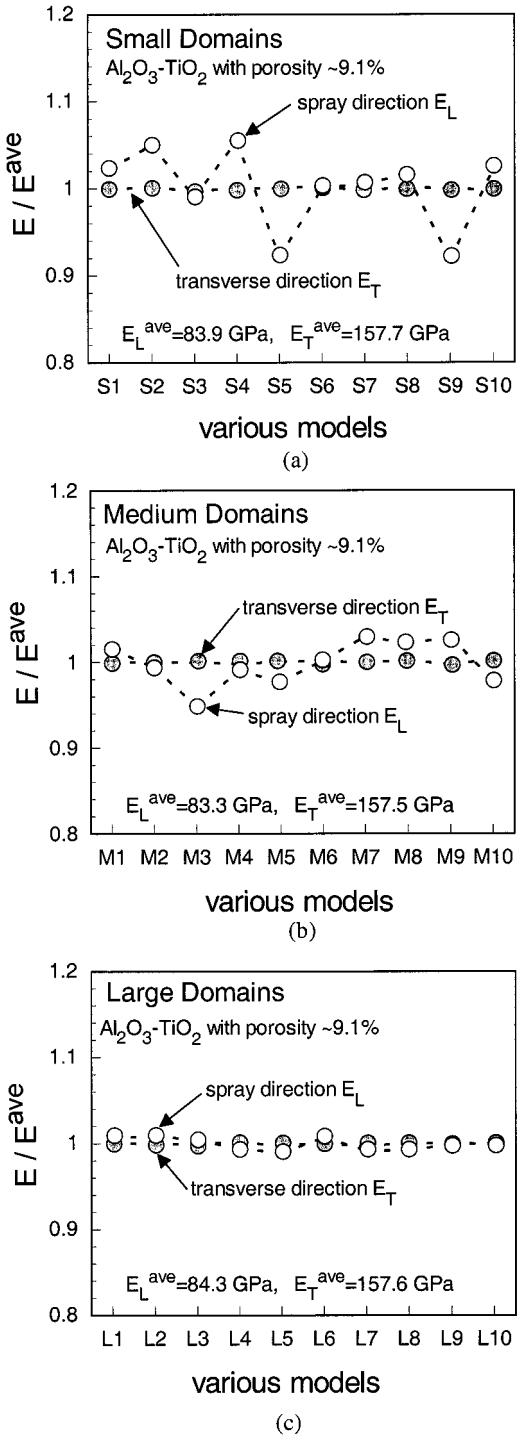

Fig. 5. Effective elastic moduli along spray direction (E_L) and transverse direction (E_T), as determined by uniaxial loading and normalized by corresponding average value (matrix modulus is E_m = 180 GPa), from (a) small-domain models, (b) medium-domain models, and (c) large-domain models (scattered E_L are observed for smaller domains).

constructed calibration curves for the force and the indented displacement. The curves were used to determine the effective moduli of porous Al_2O_3–TiO_2 models.

(2) Estimated Moduli from Indentation

Initially, the round indenter was placed on the top surface of a coating at the mid-location. Subsequently, the downward contact force was gradually increased to cause indentation into the coating. The shades of constant von Mises stress are shown in Fig. 6. Because of pores in the coating, these shades are discontinuous.

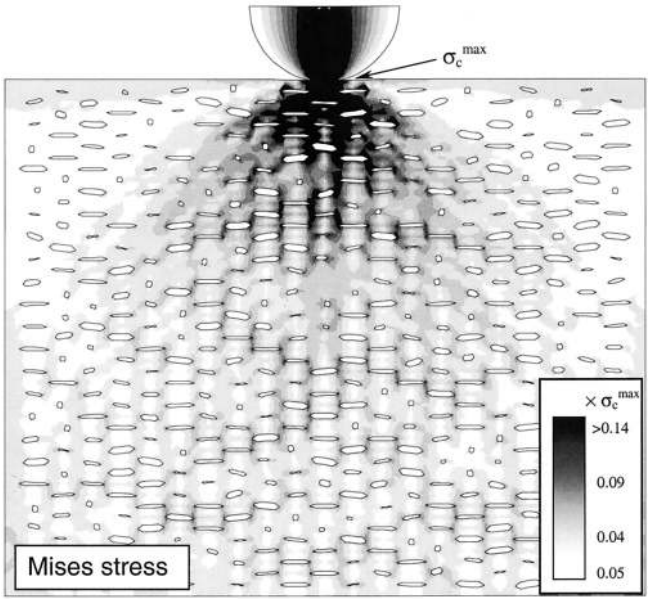

Fig. 6. Shades of constant von Mises stresses in the Al_2O_3–TiO_2 coating under round indentation. (Legend shows approximate magnitudes as fractions of the maximum contact stress, σ_c^{max}; unlike those of solid materials, shades are discontinuous because of pores.)

This result contrasts with those for solid homogeneous material, where smooth boundaries of shades are expected. Figure 6 also shows spots of high stress (darker shade) well away from the indentation caused by stress concentration resulting from the pores. To determine the modulus, the contact force (per-millimeter thickness) and the indented displacement were recorded, as shown in Fig. 7. Each curve contains a small kink caused by the contact condition over the element boundaries. Although this phenomenon can be eliminated by replacing surface elements with much finer elements, it would be difficult to do so in the special type of mesh used here. Fortunately, because the kinks occur at similar load levels, they do not influence the calculated modulus.

In experiments, elastic moduli usually are calibrated from unloading curves at a displacement of 0.5–1 μm. We chose to calculate the modulus at a displacement of 0.8 μm. Essentially, to estimate the modulus, the force at this displacement is used to calibrate the modulus from the solutions of homogeneous materials with known moduli. To measure the modulus along the transverse direction, the indenter is pressed sideways along the right boundary of each model. The estimated moduli obtained from the present indentation simulation, normalized by the uniaxial results, are shown in Fig. 8.

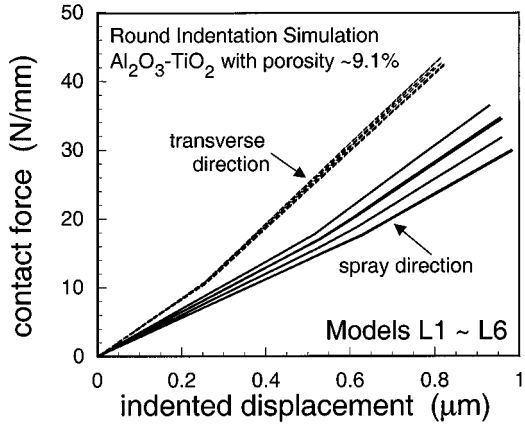

Fig. 7. Contact force versus indented displacement relations for the six Al_2O_3–TiO_2 models (*L1*–*L6*).

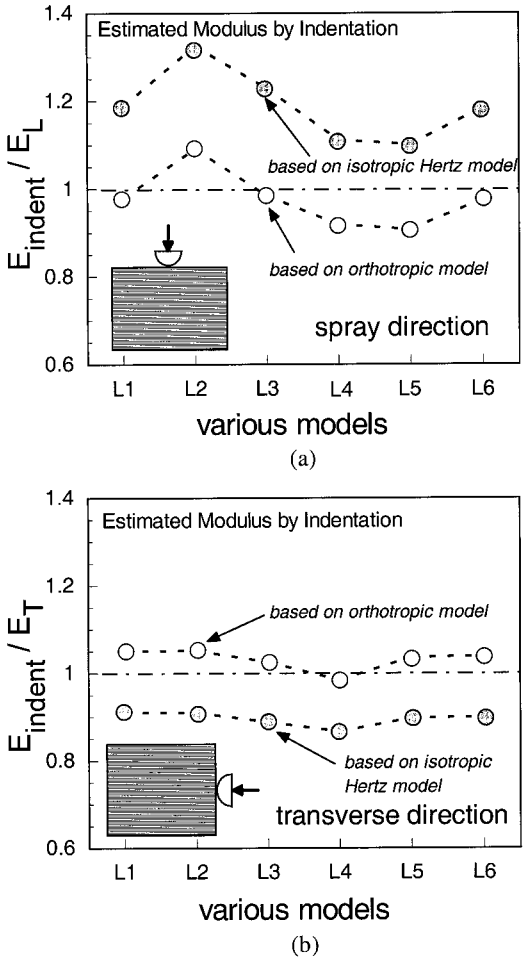

Fig. 8. Estimated elastic moduli of the six Al_2O_3–TiO_2 models, as determined from indentation simulations; results adjusted for orthotropic effects also are shown. Each modulus is normalized by the corresponding effective modulus obtained from the uniaxial test, (a) along the spray direction and (b) along the transverse direction.

To calibrate the moduli, initially, the isotropic Hertzian solutions were used as references. However, with the orthotropic factor of $E_L/E_T = 0.53$ for the Al_2O_3–TiO_2 coatings (based on the uniaxial simulations), erroneously higher E_L and lower E_T were obtained. In order to alleviate this problem, we established calibration curves based on orthotropic materials with different moduli along the spray and transverse directions. We conducted several indentation simulations for homogeneous, transversely isotropic materials with a modulus ratio of $E_L/E_T = 0.53$. Using the solutions of these models, we adjusted the moduli estimated from the contact-force-indented displacement curves, as shown in Fig. 7. Essentially, the modulus along the spray direction decreased by ~18%, while the modulus along the transverse direction increased by 15%, and the errors with respect to the moduli determined from the uniaxial test were reduced significantly. However, regardless of the calibration curves used to estimate E_L, the results showed substantial spread among the six models. In fact, the maximum difference was ~20% for the modulus along the spray direction. This difference occurred even through the overall pore size and shape distributions were identical, a result studied next.

(3) Zone of Influence

The physical factor causing the variations in the estimated modulus is the different pore morphology beneath the indent. The force displacement of the indentation is characterized by the small region, or zone of influence, below the contact surface, as illustrated in Fig. 9. Essentially, the sizes and shapes of a limited

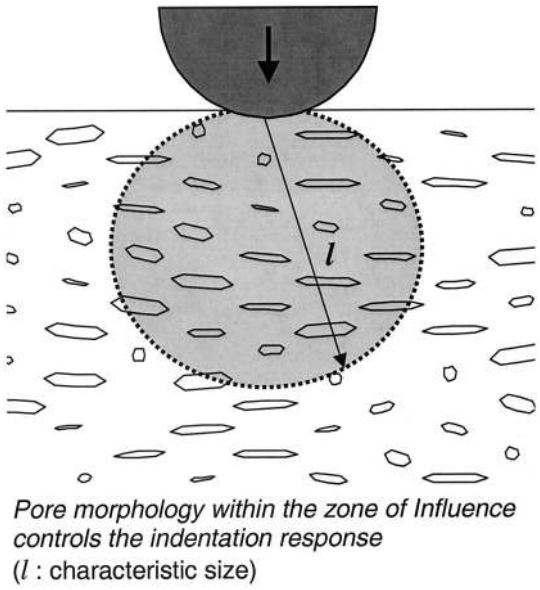

Fig. 9. Schematic showing zone of influence (shaded region) beneath contact region; pore morphology in this zone controls the response of indentation.

number of pores within this zone control the indenter response. The characteristic size of the zone should be some multiple of contact surface/length. When the indented displacement is 0.8 μm, the contact length is ~18 μm, and the characteristic size of the zone of influence is ~100 μm. Naturally, when the stress state is not uniform throughout this zone, the influence of a given pore depends on its surrounding stress magnitude. Under contact loading, the pores near the point contact should have greater influence on the indenter response.

Variations of estimated modulus occurred not only model-to-model but also within a single model. A series of nine indentation tests was conducted on Model *L*1 at various sites on its top surface, as shown by the arrows in Fig. 10(a). Here, $S = 0$ corresponds to the mid-surface of the model, and the indentation sites are separated by ~20 μm. The model is 370 μm wide, and all of the sites are located far enough away from the sides to exclude any boundary effects. The estimated spray-direction modulus, calibrated by the orthotropic model, is normalized by the E_L from the uniaxial test, as shown in Fig. 10(b). These results clearly demonstrate the local characteristics of each indentation site.

There was a spread of nearly 40% among the sites within a distance less than the indenter diameter of 100 μm. This larger variability can be attributed to the arrangements of pore locations in our models. The results shown in Fig. 8 were obtained from six different models, but all were indented at the midpoint. Because of the special type of mesh design, a column of pores always existed along the midpoint axis. Although the pore morphologies were different, this fact may have reduced the modulus variability. On the other hand, the results in Fig. 10 include indentation at surface locations, where there are no pores directly underneath. In such a case, the response can be very stiff.

VII. Conclusions

Numerical simulations of the effects of pores on the constitutive response of plasma-sprayed ceramic coatings provide valuable parametrical information on several processing variables, and that cannot be obtained easily from experiments. The results of our study clearly point out the significance of porosity and pore aspect ratio and the influence of domain sizes on the estimation of overall, or effective, modulus. The present investigation also reveals underlying causes for the inconsistent measurements often obtained by microindentation tests.

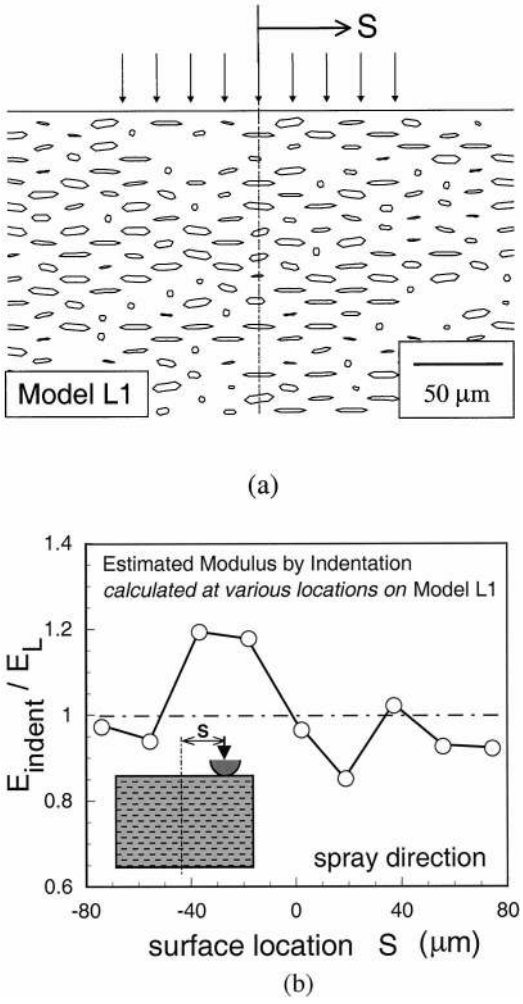

Fig. 10. (a) Arrows indicating surface locations of the indentation point on Model *L*1; pore morphology beneath each indent controls the response of indentation. (b) Estimated E_L, determined from indentation simulations; results are normalized and calibrated for the orthotropic effect.

Although the role of pore aspect ratio in influencing the stiffness of porous media is well known, the present analysis demonstrates this effect in models containing hundreds of pores with various sizes and shapes. Although not random in the mathematical sense, our models represent the aggregate result of various pore locations, sizes, shapes, and orientations. The effective moduli of those models are scattered over a wide spectrum at a given porosity. A more important aspect of these random models is that they can be used to quantify the domain-size effect on the averaging properties of coatings. The domain-size dependence must be known before any continuum models are used to analyze coatings on a structural scale. When the structural dimensions of coatings are not large enough with respect to the characteristic pore sizes, the average properties or the homogenization of the material may not yield proper solutions. In order to investigate this aspect, we modeled Al_2O_3–TiO_2 coatings with pore sizes and shape distributions following the experimentally measured pore morphology.

Our analysis revealed that nearly consistent moduli (below $\pm 5\%$) can be obtained for domain sizes $>150\ \mu m \times 150\ \mu m$. Within a smaller domain, the effective moduli may vary from domain to domain, even if the porosity and mean pore aspect ratio are identical. This minimum domain size is about an order of magnitude greater than the sizes of larger pores. In actual coatings, the minimum size may be greater, because there can be few very large pores, and some pores may be clustered. These effects can add significantly to the scattering of the average modulus. Identifying the required conditions for consistent average properties is essential in many coating analyses. Often, computational resources dictate the average properties to be used for modeling coatings on a structural scale. For example, when a coating is modeled with its substrate and other geometric features, the overall dimensions may be >1 mm. On this size scale, many individual pores (2–20 μm) are too small and complex to be included in the entire model, and the coating must be modeled as a homogeneous material. For such a problem, one must ensure that the effects of individual pores (which are ignored in a homogeneous model) do not play a significant role in the stress and deformation fields of the coating.

In the simulations of the indentation test, we have identified the source of variation in the measurements. The large scattering of the estimated modulus can result from the different pore morphologies within the zones of influence below the contact. In order to obtain an accurate modulus, several indentation measurements should be conducted at various locations, and the average modulus must be used. Furthermore, the sprayed coatings may require solutions from orthotropic models before the moduli measurements can be calibrated properly.

Acknowledgments

The computations were conducted on an HP7000/C180 workstation, using the finite-element code ABAQUS, which was made available under academic license from Hibbitt, Karlson, and Sorenson, Inc., Providence, RI.

References

[1]S. H. Leigh and C. C. Berndt, "Quantitative Evaluation of Void Distributions within a Plasma-Sprayed Ceramic," *J. Am. Ceram. Soc.*, **82** [1] 17–21 (1999).
[2]G. Montavon, S. Sampath, C. C. Berndt, H. Herman, and C. Coddet, "Effects of Vacuum Plasma Spray Processing Parameters on Splat Morphology," *J. Therm. Spray Technol.*, **4**, 67–74 (1995).
[3]P. Bengtsson and T. Johannesson, "Characterization of Microstructural Defects in Plasma-Sprayed Thermal Barrier Coatings," *J. Therm. Spray Technol.*, **4**, 245–51 (1995).
[4]J. H. Harding, P. A. Mulheran, S. Cirolini, M. Marchese, and G. Jacucci, "Modeling of the Deposition Process of Thermal Barrier Coatings," *J. Therm. Spray Technol.*, **4**, 34–40 (1995).
[5]Y. H. Zhao, G. P. Tandon, and G. J. Weng, "Elastic Moduli for a Class of Porous Materials," *Acta. Mech.*, **76**, 105–30 (1989).
[6]Y. H. Zhao and G. J. Weng, "Effective Elastic Moduli of Ribbon-Reinforced Composites," *J. Appl. Mech.*, **57**, 158–67 (1990).
[7]J. Argyris, I. St. Doltsinis, M. Eggers, and R. Handel, "Studies on Ceramic Coatings, Deduction of Mechanical and Thermal Properties from the Microstructure of the Material," *Comp. Meth. Appl. Mech. Eng.*, **111**, 203–34 (1994).
[8]M. Kachanov, I. Tsukrov, and B. Shafiro, "Effective Moduli of Solids with Cavities of Various Shapes," *Appl. Mech. Rev.*, **47**, S151–S174 (1994).
[9]M. Kachanov, "Elastic Solids with Many Cracks: A Simple Method of Analysis," *Int. J. Solids Struct.*, **23**, 23–43 (1987).
[10]Z. Hashin, "The Differential Scheme and Its Application to Cracked Materials," *J. Mech. Phys. Solids.*, **36**, 719–34 (1988).
[11]R. M. Christensen, "A Critical Evaluation for a Class of Micromechanical Models," *J. Mech. Phys. Solids*, **38**, 379–404 (1990).
[12]T. Nakamura and S. Suresh, "Effects of Thermal Residual Stresses and Fiber Packing on Deformation of Metal-Matrix Composites," *Acta Metall. Mater.*, **41**, 1665–81 (1993).
[13]N. Ramakrishnan and V. S. Arunachalam, "Effective Elastic Moduli of Porous Ceramic Materials," *J. Am. Ceram. Soc.*, **76**, 2745–52 (1993).
[14]A. R. Boccaccini, "Comment on Effective Elastic Moduli of Porous Ceramic Materials," *J. Am. Ceram. Soc.*, **77**, 2779–81 (1994).
[15]M. E. Coles, R. D. Hazlett, E. L. Muegge, K. W. Jones, B. Andrews, B. Dowd, P. Siddons, A. Peskin, P. Spanne, and W. E. Soll, "Developments in Synchrotron X-ray Microtomography with Applications to Flow in Porous Media"; pp. 413–24 in *Proceedings of the SPE Annual Technical Conference and Exhibition*. Society of Petroleum Engineers, Dallas, TX, 1998.
[16]S. R. J. Saunders, "Measurement Methods in Surface Engineering," *Surf. Eng.*, **9**, 293–99 (1993).
[17]K. Matsushita, S. Kuratani, T. Okamoto, and M. Shimada, "Young's Modulus and Internal Friction in Alumina Subjected to Thermal Shock," *J. Mater. Sci. Lett.*, **3**, 345–48 (1984).
[18]R. McPherson and P. Cheang, "Elastic Anisotropy of APS Alumina Coatings and Its Relationship to Microstructure"; pp. 277–90 in *High Performance Ceramic Films and Coatings*. Edited by P. Vincenzini. Elsevier Science, New York, 1991.
[19]S. H. Leigh and C. C. Berndt, "Elastic Response of Thermal-Spray Deposits under Indentation Tests," *J. Am. Ceram. Soc.*, **80**, 2093–99 (1997). □